

Article

Morphology Control of Nanocrystallized C₆₀ Thin Films Prepared by Poor Solvent Immersion

Kazuki Umemoto¹, Masaki Takeda¹, Yuki Tezuka¹, Miho Doi¹, Bozhang Lyu¹ and Akito Masuhara^{1,2,*}

¹ Graduate School of Science and Engineering, Yamagata University, 4-3-16 Jonan, Yonezawa, Yamagata 992-8510, Japan; tsr16867@st.yamagata-u.ac.jp (K.U.); thr99823@st.yamagata-u.ac.jp (M.T.); tda60518@st.yamagata-u.ac.jp (Y.T.); tdw83631@st.yamagata-u.ac.jp (M.D.); tht79494@st.yamagata-u.ac.jp (B.L.)

² Research Center for Organic Electronics (ROEL), Yamagata University, 4-3-16 Jonan, Yonezawa, Yamagata 992-8510, Japan

* Correspondence: masuhara@yz.yamagata-u.ac.jp; Tel.: +81-238-26-3891

Received: 2 May 2018; Accepted: 18 May 2018; Published: 20 May 2018



Abstract: Nanocrystallized C₆₀ thin films of such as hexagonal, plate-like, and rod-like morphologies were recrystallized by poor solvent immersion, employing 1-propanol, 2-propanol, and butanol respectively. A C₆₀ thin film fabricated by evaporation was immersed in the poor solvent, partially dissolving the surface C₆₀. This was followed by the solvent rapidly reaching a supersaturated state, resulting in the induced recrystallization of the C₆₀. C₆₀ fine high-density crystals were successfully prepared using propanol, with crystal sizes varying between 84 and 141 nm by changing the immersion time. In addition, due to the 1-propanol recrystallizing solvated crystals which were formed through interactions between the solvent and the C₆₀, uniform C₆₀ fine crystals were obtained by the formation of a large number of nucleation sites.

Keywords: C₆₀; thin film; recrystallization; solvent immersion; morphology control; solvated crystal

1. Introduction

Organic semiconductor materials in the form of fullerenes have been intensively studied as attractive materials for various state-of-art devices such as field effect transistors [1], light emitting diodes [2], chemical sensors [3], photodetectors [4], and solar cells [5]. In several kinds of fullerenes, C₆₀ shows promising optoelectronic properties [6–8] that are expected to be developed further. Crystallization of C₆₀ and control of the morphology of their crystals is one of the approaches currently used in order to enhance these properties, and the morphology control of fine crystals has revealed novel optoelectronic properties that depend on crystal sizes and shapes [9–11]. In terms of the applications of C₆₀ for various optoelectronic devices, morphology control of C₆₀ fine crystals in thin film state enables control of nanostructures, which can improve device performances. In particular, approaches of morphology control through use of solutions are required for various optoelectronic devices that necessitate cost-effective process and higher device performance [12].

Several techniques have been developed to control the morphologies of C₆₀ fine crystals without the demanding requirements of using templates, special equipment, high temperature, or high pressure. Using liquid-phase synthesis to obtain C₆₀ fine crystals following the method of liquid-liquid interface precipitation [13] and reprecipitation [14] is one of the simplest techniques. These techniques can transform the morphologies of C₆₀ fine crystals simply by changing the solvents used for recrystallizing the C₆₀ molecules [15,16]; however, multiple steps are required to fabricate nanocrystallized C₆₀ thin films and it is difficult to achieve precise control of nanostructures in a film state. To develop a method

that overcomes these obstacles, several studies report using as-deposited C₆₀ thin films to control the morphologies of C₆₀ fine crystals. Kim et al. demonstrated C₆₀ nanowires on a substrate, which were prepared by solvent vapor annealing (SVA) using good solvents to recrystallize C₆₀ molecules, where their growth direction was controlled in vertical and lateral directions by adjusting Marangoni flows [17]. Nojiri et al. also fabricated a nanocrystallized C₆₀ thin film prepared by SVA, using an as-deposited C₆₀ thin film. This film improved charge transport ability of a C₆₀ layer and power conversion efficiency from 1.8% to 2.1%, which was found to enhance solar cell performances [18]. These studies have shown that employing an as-deposited C₆₀ thin film is a useful strategy for forming nanocrystallized C₆₀ thin films via the recrystallization of C₆₀.

In this work, we propose the poor solvent immersion to control the morphologies of nanocrystallized C₆₀ thin films using as-deposited C₆₀ thin film. These morphologies, such as hexagonal, plate-like, and rod-like, were successfully controlled by employing optimal poor solvents such as 1-propanol, 2-propanol, and butanol, respectively. In particular, 1-propanol formed uniform 84–141 nm size C₆₀ fine crystals with high density through specific recrystallization process via solvation in this system. Poor solvent immersion simply formed nanocrystallized C₆₀ thin films and it has potential application in versatile materials enabling them to control nanostructures.

2. Materials and Methods

2.1. Materials

C₆₀ powder (99.9%) was purchased from Tokyo Chemical Industry (TCI) (Tokyo, Japan). Methanol (99.8%), ethanol (99.5%), 1-propanol (99.5%), 2-propanol (99.7%), butanol (99.0%), hexane (96.0%), cyclohexane (98.0%), and chloroform (99.0%) were used to recrystallize as-deposited C₆₀ thin films and purchased from TCI (Tokyo, Japan).

2.2. Fabrication of Nanocrystallized C₆₀ Thin Film

100 nm C₆₀ thin films was thermally evaporated onto the ITO substrate at a pressure of 2×10^{-4} Pa. As-deposited C₆₀ thin films were immersed into 15.0 mL various organic solvents in a plate. After immersion, nanocrystallized C₆₀ thin films were dried for 12 h at room temperature (under ambient atmosphere).

2.3. Characterization of Nanocrystallized C₆₀ Thin Film

X-ray diffraction (XRD) patterns of the samples were measured on a Smart Lab (Rigaku, Tokyo, Japan) (using Cu K α radiation at 45 kV and 200 mA). The samples were observed by a JSM-6700F scanning electron microscope (SEM) (Japan Electron Optics Laboratory (JEOL), Tokyo, Japan) (accelerating voltage of 10 kV). Visible absorption spectra of the samples were obtained on a V-670 spectrophotometer (Japan Spectroscopic Corporation (JASCO), Tokyo, Japan) (detecting wavelength range of 200 to 800 nm).

3. Results and Discussion

3.1. Poor Solvent Immersion

Figure 1 shows a schematic illustration of poor solvent immersion. In this method, a thermally evaporated C₆₀ thin film is immersed in a poor solvent and the surface morphologies are controlled by the recrystallization of C₆₀. When an as-deposited C₆₀ thin film is immersed in a poor solvent, the C₆₀ on the surface is partially dissolved. The solvent rapidly reaches a state of supersaturation because of its inability to dissolve large amounts of C₆₀, and so recrystallization takes place at the surface of the C₆₀ thin film followed by the formation of well-controlled C₆₀ fine high-density crystals, which can induce a transformation in their morphologies in the thin film state.

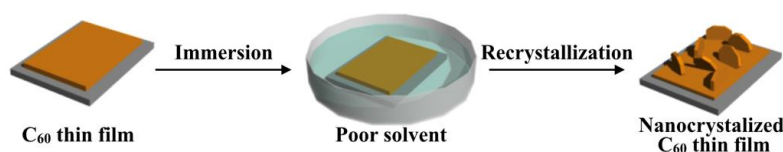


Figure 1. Schematic illustration of morphology control of the nanocrystallized C₆₀ thin films prepared by poor solvent immersion.

3.2. Optimization of Poor Solvent

To determine the optimal solvent for recrystallizing C₆₀ and controlling its morphology, various organic solvents such as methanol, ethanol, propanol, butanol, hexane, cyclohexane, and chloroform were tested. When the alcohol solvents (except for methanol and ethanol) were used, a large number of C₆₀ fine crystals on thin films immersing for 60 min were observed in the scanning electron microscope (SEM) images shown in Figure 2. An extremely poor solvent such as methanol (0.000 mg/mL [19], Supplementary Materials Table S1) does not affect the surface morphology (Figure S1a) as significantly when compared to a C₆₀ thin film fabricated through deposition by evaporation. Although ethanol is used as a treatment solvent in SVA and induces the recrystallization of C₆₀ due to its low solubility (0.001 mg/mL, Table S1) [19], C₆₀ fine crystals on thin film have lower density (Figure S1b) compared to the nanocrystallized C₆₀ thin films recrystallized by propanol. In general, C₆₀ is insoluble in polar solvents such as these, but C₆₀ tends to increase solubility by increasing the number of carbon atoms in the solvents [19,20]. Butanol notably shows this tendency and forms 1 μm-sized rod-like C₆₀ fine crystals due to increasing solubility and, as a result, the morphologies are drastically changed. However, recrystallized C₆₀ fine crystals on the thin film are relatively low-density, and the SEM image (Figure 2d) shows cracks which severely damage the state of the thin film and represent an obstacle to application in various optoelectronic devices. Conversely, weak polar solvents at a certain level of solubility, such as hexane (0.043 mg/mL), cyclohexane (0.036 mg/mL), and chloroform (0.16 mg/mL), dissolve a large amount of C₆₀ from thin films such that they do not induce recrystallization (Figure S1c–e, Table S1) [19]. According to experimental SEM observations, propanol recrystallized uniform C₆₀ fine crystals on thin films with high density, so this was identified as the key solvent for controlling the morphologies of nanocrystallized C₆₀ thin films. Interestingly, it is found that although 1-propanol and 2-propanol contain the same number of carbons, the resulting morphologies are significantly different. 1-propanol forms 300 nm sized C₆₀ fine crystals with uniform size and shape, while 2-propanol, a structural isomer of 1-propanol, forms 500 nm–1 μm-sized C₆₀ fine crystals.

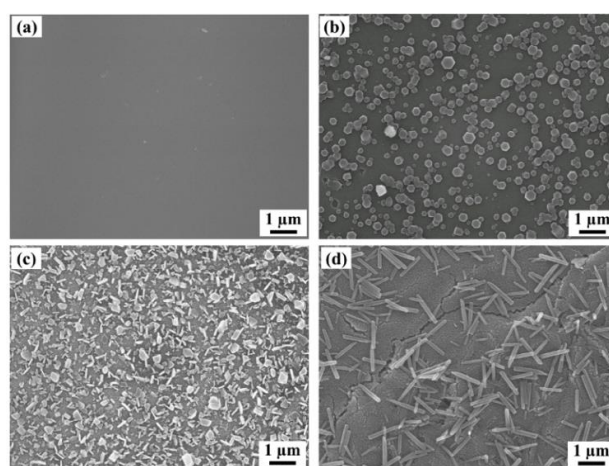


Figure 2. SEM images of (a) a thermally evaporated C₆₀ thin film and (b) hexagonal, (c) plate-like, and (d) rod-like C₆₀ fine crystals on the films prepared by immersion in 1-propanol, 2-propanol, and butanol as a poor solvent for 60 min, respectively.

3.3. Crystal Structure

To explore the most significant factors that contribute to structural differences, we measured the crystal structures of the nanocrystallized C_{60} thin films prepared with 1-propanol and 2-propanol using X-ray diffraction (XRD) analysis, as shown in Figure 3. A nanocrystallized C_{60} thin film recrystallized by 2-propanol shows diffraction peaks at $2\theta = 10.4, 17.6, 20.7$, which is consistent with an XRD pattern of as-deposited C_{60} thin film and corresponds to a typical face-centered cubic (fcc) C_{60} crystal structure [21]. The other film, recrystallized by 1-propanol instead of 2-propanol, clearly exhibits a diffraction peak at $2\theta = 19.2$, which is not detected for the as-deposited C_{60} film. This suggests 1-propanol forms a different crystal structure to the FCC structure of a nanocrystallized C_{60} thin film prepared by 2-propanol. Our previous study on C_{60} fine crystals prepared by the reprecipitation method found that C_{60} interacts and cocrystallizes with various solvents, resulting in the formation of solvated crystals that incorporate the solvent [21]. Moreover, studying the phase transformation of C_{60} fine crystals and the associated change of their shapes induced by the exchanging of incorporated solvents revealed that the solvated crystals had a hexagonal crystal structure [22]. As a nanocrystallized C_{60} thin film recrystallized by 1-propanol shows a diffraction peak at $2\theta = 19.2$, this exhibits that 1-propanol interacts with C_{60} and forms solvated crystals. It is well known that C_{60} can be occupied with versatile chemical species such as alkali metal atoms, halogen molecules, and small hydrocarbon molecules, as well as solvent molecules. The intercalation of solvent into the lattice of C_{60} minimizes the lattice energy and forms various crystal shapes [23]. It assumes that solvated crystals are formed because of 1-propanol has lower steric hindrance than 2-propanol. However, this may need further study. It can therefore be considered that the solvation is a significant factor for obtaining uniformly sized C_{60} fine crystals on thin films.

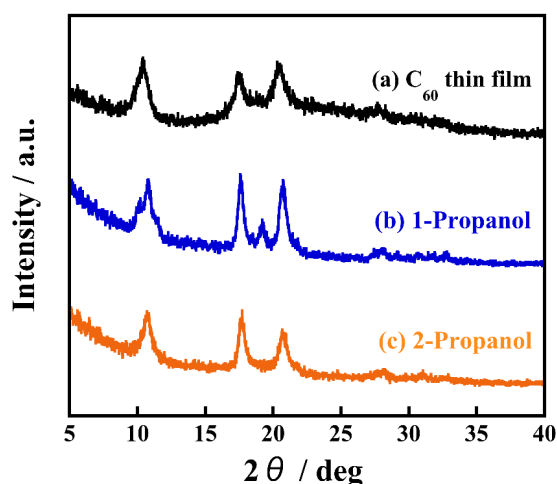


Figure 3. XRD patterns of (a) a thermally evaporated C_{60} thin film and (b) hexagonal, (c) plate-like nanocrystallized C_{60} thin films prepared by using 1-propanol and 2-propanol as a poor solvent, respectively.

3.4. Recrystallization Using 1-Propanol

To investigate the effect of solvation by 1-propanol on the formation of uniform C_{60} fine crystals, we also recorded time-resolved observation of the recrystallization process of C_{60} fine crystals during the immersion. Figure 4 shows SEM images of nanocrystallized C_{60} thin films and their crystal size distributions when immersed for 1 min, 5 min, and 30 min. From SEM observation, it is clearly seen that average crystal sizes increased to 84 ± 35 nm, 100 ± 19 nm, and 141 ± 39 nm with increasing immersion times. Interestingly, even with an immersion time as short as 1 min (corresponding to Figure 5a and Figure S2a), a large number of small-sized C_{60} fine crystals are observed. Based on these observations of real-time crystal growth, it appears that when C_{60} thin film fabricated through an

evaporation method is immersed in 1-propanol, the solution immediately reaches a supersaturation state because 1-propanol forms solvated crystals with the C_{60} molecules, which results in the immediate formation of a large number of nucleation sites in the thin film. Consequently, a large number of nuclei grow in this proposed process forming uniform solvated C_{60} fine crystals with high-density in thin film. In addition, time-resolved ultraviolet and visible absorption spectra of the nanocrystallized C_{60} thin films revealed that the absorbance at 268 nm decreased with increasing immersion times, as plotted in Figure 5b. The absorption peak at 268 nm, which corresponds to electron transfer from g_g to t_{2u} [24], rapidly decreased after immersion for 1 min. It can be deduced that 1-propanol accelerates the recrystallization of C_{60} due to solvation, resulting in a decrease of the absorbance originating from an individual C_{60} molecule. These results give evidence for the proposed recrystallization process taking place through the formation of a large number of nuclei and solvation, which is a significant step forward for recrystallizing C_{60} fine crystals with uniform size.

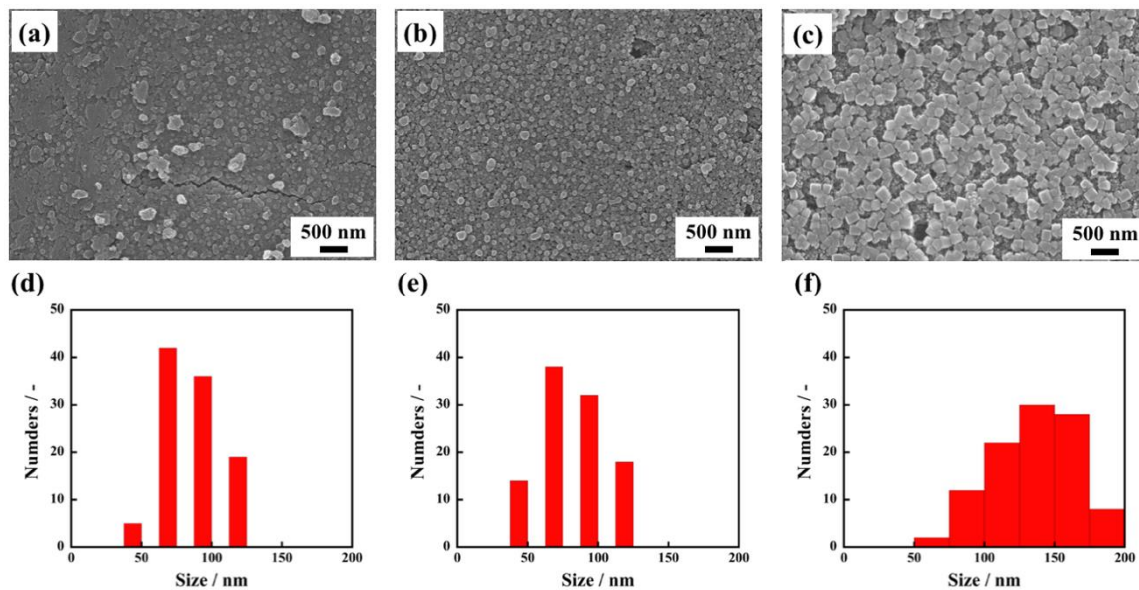


Figure 4. SEM images of nanocrystallized C_{60} thin films immersed in 1-propanol for 1 min. (a), 5 min. (b), 30 min (c), and the size distributions of C_{60} fine crystals recrystallized for 1min (d), 5 min (e), 30 min (f).

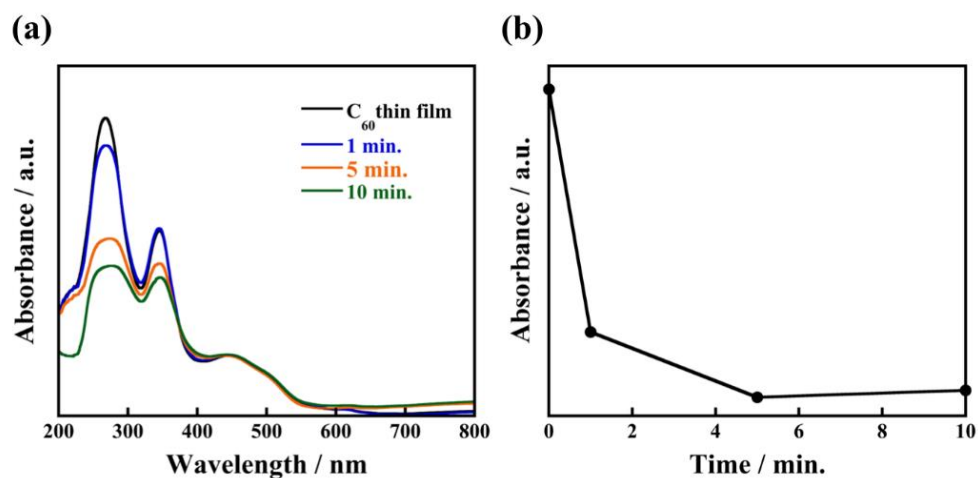


Figure 5. Absorption spectra of nanocrystallized C_{60} thin films immersed in 1-propanol for 1 min, 5 min, 10 min (a) and the relationship between absorbance at wavelength of 268 nm and immersion times (b).

3.5. Recrystallization Using 2-Propanol

In contrast, when an as-deposited C_{60} film is immersed in 2-propanol for 1 min, C_{60} fine crystals are not observed in Figure 6a. After immersion for 5 min, a small number of C_{60} fine crystals are formed, which grow to a size in the range of 500 nm–1 μm with plate-like morphology after being immersed for 30 min. From such non-uniformity of crystal size and the small number of crystals compared to the case of 1-propanol, the recrystallization process using 2-propanol is clearly different. Considering that 2-propanol does not cocrystallize with C_{60} , we propose the following model of the recrystallization process: When an as-deposited C_{60} thin film is immersed in 2-propanol, dissolution of C_{60} from the surface is dominant. After sufficient dissolution, 2-propanol slowly reaches the supersaturation state ((slower than 1-propanol) so only a small number of nuclei are formed. As a result, the C_{60} fine crystals are recrystallized with non-uniform size. XRD patterns of the nanocrystallized C_{60} thin film (Figure S3) show that the diffraction peaks almost disappear after immersion for 1 min, which suggests dissolution of C_{60} from the thin film is dominant during this time. After immersion for 5 min, distinct XRD peaks reappear due to the recrystallization of C_{60} . The absorption peak at 268 nm rapidly decreases after immersion for 5 min as shown in Figure 7, which indicates that the dissolved C_{60} is supplied for recrystallization on the surface of the nanocrystallized C_{60} thin film. These results support our proposed model of the recrystallization process in 2-propanol which, due to the dissolution process taking a finite amount of times, takes longer to reach supersaturation state than 1-propanol, resulting in the formation of non-uniform C_{60} fine crystals with non-uniform size.

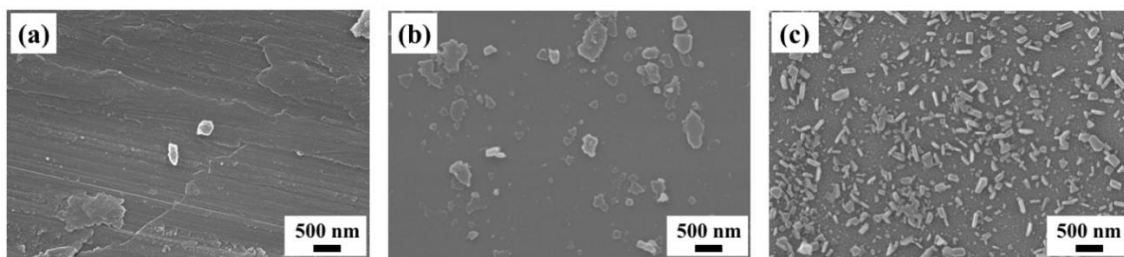


Figure 6. SEM images of nanocrystallized C_{60} thin films immersed in 1-propanol for (a) 1 min, (b) 5 min, (c) 30 min.

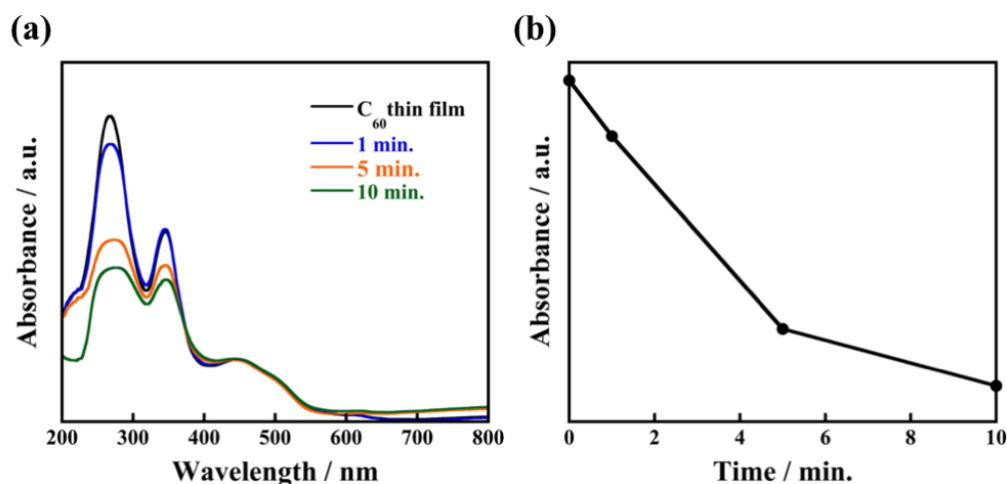


Figure 7. Absorption spectra of nanocrystallized C_{60} thin films immersed in 2-propanol for 1 min, 5 min, 10 min (a) and the relationship between absorbance at wavelength of 268 nm and immersion times (b).

4. Conclusions

Nanocrystallized C₆₀ thin films with hexagonal, plate-like, and rod-like morphologies were successfully prepared by poor solvent immersion. Uniform average crystal sizes could be controlled between 84 and 141 nm by changing immersion times and using 1-propanol as the poor solvent. Due to the 1-propanol interacting with C₆₀ molecules, uniform C₆₀ fine crystals were recrystallized in a thin film via a proposed mechanism associated with the formation of solvated crystals. Size- and shape-controlled synthesis of C₆₀ fine crystals on thin film state by poor solvent immersion can therefore provide an appropriate synthetic route to producing optoelectronic materials.

Supplementary Materials: The following are available online at <http://www.mdpi.com/2227-7080/6/2/51/s1>, Figure S1: SEM images of the C₆₀ thin film immersed using (a) methanol, (b) ethanol, (c) hexane, (d) cyclohexane, and (e) chloroform for 60 min, respectively; Figure S2: High magnification SEM images of nanocrystallized C₆₀ thin films immersed in 1-propanol for 1 min (a), 5 min (b), (c) 30 min, and C₆₀ thin films immersed in 2-propanol for (d) 1 min, (e) 5 min, (f) 30 min; Figure S3: XRD patterns of (a) a thermally evaporated C₆₀ thin film and nanocrystallized C₆₀ thin film immersed in 1-propanol for (b) 1 min, (c) 5 min, (d) 10 min, (e) 30 min, respectively; Table S1: Solubility of C₆₀ in various solvents.

Author Contributions: Conceptualization, A.M.; Methodology, A.M.; K.U.; M.T.; Y.T.; B.L.; Formal Analysis, M.T.; M.D.; Writing Original Draft Preparation, K.U.; Writing Review and Editing, K.U.; A.M.; Supervision, A.M.; Funding Acquisition, A.M.; All authors have read and approved the final manuscript.

Funding: This work was partially supported by a research grant from The Cosmetology Research Foundation, Japan Society for the Promotion of Science KAKENHI Grant Number JP 18K04805.

Acknowledgments: The authors are very grateful to Atsushi Ito for supporting and valuable discussion on this work.

Conflicts of Interest: The authors declare no conflict of interest.

References

1. Ohashi, H.; Tanigaki, K.; Kumashiro, R.; Sugihara, S.; Hiroshiba, S.; Kimura, S.; Kato, K.; Takata, M. Low-glancing-angle X-ray diffraction study on the relationship between crystallinity and properties of C₆₀ field effect transistor. *Appl. Phys. Lett.* **2004**, *84*, 520–522. [[CrossRef](#)]
2. Lee, J.Y. Efficient hole injection in organic light-emitting diodes using C₆₀ as a buffer layer for Al reflective anodes. *Appl. Phys. Lett.* **2006**, *88*, 073512. [[CrossRef](#)]
3. Lin, H.-B.; Shih, J.-S. Fullerene C₆₀-cryptand coated surface acoustic wave quartz crystal sensor for organic vapors. *Sens. Actuators B Chem.* **2003**, *92*, 243–254. [[CrossRef](#)]
4. Tsai, W.-W.; Chao, Y.-C.; Chen, E.-C.; Zan, H.-W.; Meng, H.-F.; Hsu, C.-S. Increasing organic vertical carrier mobility for the application of high speed bilayered organic photodetector. *Appl. Phys. Lett.* **2009**, *95*, 213308. [[CrossRef](#)]
5. Sariciftci, N.-S.; Smilowitz, L.; Heeger, A.-J.; Wudl, F. Photoinduced Electron Transfer from a Conducting Polymer to Buckminsterfullerene. *Science* **1992**, *258*, 1474–1476. [[CrossRef](#)] [[PubMed](#)]
6. Akada, M.; Hirai, T.; Takeuchi, J.; Yamamoto, T.; Kumashiro, R.; Tanigaki, K. Superconducting phase sequence in R_x C₆₀ fullerides (R=Smand Yb). *Phys. Rev. B* **2006**, *73*, 632–636. [[CrossRef](#)]
7. Guldi, D.M.; Prato, M. Excited-State Properties of C₆₀ Fullerene Derivatives. *Acc. Chem. Res.* **2000**, *33*, 695–703. [[CrossRef](#)] [[PubMed](#)]
8. Peumans, P.; Uchida, S.; Forrest, S.-R. Efficient bulk heterojunction photovoltaic cells using small-molecular-weight organic thin films. *Nature* **2003**, 1–5. [[CrossRef](#)] [[PubMed](#)]
9. Miyazawa, K.; Kuwasaki, Y.; Hamamoto, K.; Nagata, S.; Obayashi, A.; Kuwabara, M. Structural characterization of C₆₀nanowhiskers formed by the liquid/liquid interfacial precipitation method. *Surf. Interface Anal.* **2003**, *35*, 117–120. [[CrossRef](#)]
10. Kizuki, T. Chapter 8 in *Situ Transmission Electron Microscopy of Fullerene Nanowhiskers and Related Carbon Nanomaterials*. In *Fullerene Nanowhiskers*, 1st ed.; Miyazawa, K., Tachibana, M., Mashino, T., Kizuka, T., Ochiai, Y., Eds.; Pan Stanford Publishing Pte., Ltd.: Singapore, 2011; pp. 103–116.
11. Matsuishi, K. Chapter 11 Optical Properties of Fullerene Nanowhiskers. In *Fullerene Nanowhiskers*, 1st ed.; Miyazawa, K., Tachibana, M., Mashino, T., Kizuka, T., Ochiai, Y., Eds.; Pan Stanford Publishing Pte., Ltd.: Singapore, 2011; pp. 147–162.

12. Thomas, M.; Worfolk, B.J.; Rider, D.A.; Taschuk, M.T.; Buriak, J.M.; Brett, M.J. C₆₀ Fullerene Nanocolumns-Polythiophene Heterojunctions for Inverted Organic Photovoltaic Cells. *ACS Appl. Mater. Interfaces* **2011**, *3*, 1887–1894. [[CrossRef](#)] [[PubMed](#)]
13. Sathish, M.; Miyazawa, K. Size-Tunable Hexagonal Fullerene (C₆₀) Nanosheets at the Liquid-Liquid Interface. *J. Am. Chem. Soc.* **2007**, *129*, 13816–13817. [[CrossRef](#)] [[PubMed](#)]
14. Kasai, H.; Nalwa, H.S.; Oikawa, H.; Okada, S.; Matsuda, H.; Minami, N.; Kakuta, A.; Ono, K.; Mukoh, A.; Nakanishi, H. Novel Preparation Method of Organic Microcrystals. *Jpn. J. Appl. Phys.* **1992**, *31*, L1132–L1134. [[CrossRef](#)]
15. Miyazawa, K. Chapter 1 Introduction of Fullerene Nanowhiskers. In *Fullerene Nanowhiskers*, 1st ed.; Miyazawa, K., Tachibana, M., Mashino, T., Kizuka, T., Ochiai, Y., Eds.; Pan Stanford Publishing Pte., Ltd.: Singapore, 2011; pp. 1–23.
16. Masuhara, A.; Tan, Z.; Kasai, H.; Nakanishi, H.; Okikawa, H. Chapter 7 Fabrication and Characterization of C₆₀ Fine Crystals and Their Hybridization. In *Fullerene Nanowhiskers*, 1st ed.; Miyazawa, K., Tachibana, M., Mashino, T., Kizuka, T., Ochiai, Y., Eds.; Pan Stanford Publishing Pte., Ltd.: Singapore, 2011; pp. 89–101.
17. Kim, J.; Park, C.; Park, J.E.; Chu, K.; Choi, H.C. Vertical Crystallization of C₆₀ Nanowires by Solvent Vapor Annealing Process. *ACS Nano* **2013**, *7*, 9122–9128. [[CrossRef](#)] [[PubMed](#)]
18. Nojiri, K.; Shahiduzzaman, M.; Yamamoto, K.; Kuwabara, T.; Takahashi, K.; Taima, T. Interpenetrating heterojunction photovoltaic cells based on C₆₀ nano-crystallized thin films. *Org. Electron.* **2016**, *38*, 107–114. [[CrossRef](#)]
19. Ruoff, R.S.; Tse, D.S.; Malhotra, R.; Lorents, D.C. Solubility of fullerene (C₆₀) in a variety of solvents. *J. Phys. Chem.* **1993**, *97*, 3379–3383. [[CrossRef](#)]
20. Hansen, C.M.; Smith, A.L. Using Hansen solubility parameters to correlate solubility of C₆₀ fullerene in organic solvents and in polymers. *Carbon* **2004**, *42*, 1591–1597. [[CrossRef](#)]
21. Masuhara, A.; Tan, Z.; Ikeshima, M.; Sato, T.; Kasai, H.; Oikawa, H.; Nakanishi, H. Cyclic transformation in shape and crystal structure of C₆₀ microcrystals. *CrystEngComm* **2012**, *14*, 7787–7791. [[CrossRef](#)]
22. Tan, Z.; Masuhara, A.; Kasai, H.; Nakanishi, H.; Oikawa, H. Thermal-induced shape transformation of solvated C₆₀ microcrystals. *Carbon* **2013**, *64*, 370–376. [[CrossRef](#)]
23. Park, C.; Park, J.E.; Choi, H.C. Crystallization-Induced Properties from Morphology-Controlled Organic Crystals. *Acc. Chem. Res.* **2014**, *47*, 2353–2364. [[CrossRef](#)] [[PubMed](#)]
24. Graja, A.; Farges, J.-P. Optical spectra of C₆₀ and C₇₀ complexes: Their similarities and differences. *Adv. Mater. Opt. Electron.* **1998**, *8*, 215–228. [[CrossRef](#)]



© 2018 by the authors. Licensee MDPI, Basel, Switzerland. This article is an open access article distributed under the terms and conditions of the Creative Commons Attribution (CC BY) license (<http://creativecommons.org/licenses/by/4.0/>).